International Journal of Heat and Technology
Vol. 43, No. 1, February, 2025, pp. 76-84
Journal homepage: http://iieta.org/journals/ijht

Hydration Heat Kinetics and Temperature Control in Ultra-Large Volume Concrete: A Case Study

Jinglei Han[1], Guoping Zhang[1], Peng Jia[2*], Zhaohan Nie[3], Changsong Zhao[3], Xiaoye Liu[4]

[1] Project Management Office for the Second Section of the Jinan Fenghuang Road North Extension Project, CCCCSHEC Fourth Engineering Company Ltd., Wuhu 241009, China
[2] Technical Center Department Planning, Jinan Rail Transit Group Co., Ltd., Jinan 250000, China
[3] School of Civil Engineering, Shandong Jiaotong University, Jinan 250357, China
[4] School of Science, Shandong Jiaotong University, Jinan 250357, China

Corresponding Author Email: jiapeng1984@163.com

https://doi.org/10.18280/ijht.430109

Received: 2 August 2024
Revised: 15 December 2024
Accepted: 28 December 2024
Available online: 28 February 2025

Keywords:
large volume concrete, heat of hydration, temperature, stress distribution, cracking

ABSTRACT

Uneven temperature rise in large concrete structures, caused by cement hydration heat, can lead to thermal stress concentration, resulting in early cracking. This, in turn, affects the structure's functionality, durability, and overall integrity. To address this issue, this study focuses on the Jinan Yellow River Fenghuang Bridge in China, analyzing the hydration heat kinetics of ultra-large volume concrete and exploring temperature control measures. It also investigates the distribution patterns of temperature and stress in the joint section and foundation slab across different seasons. The findings reveal that in colder seasons, the temperature stress in the first layer of the joint section fluctuates significantly with age, strongly influenced by hydration heat. In contrast, during warmer seasons, the early-stage stress in the foundation slab is relatively low, but it increases rapidly in later stages. Therefore, temperature control measures need to be optimized to mitigate stress risks. Experimental and numerical simulation results show strong consistency, with errors not exceeding 5%, confirming the accuracy and reliability of the model. Based on these insights, the study proposes strategies for real-time monitoring, automatic early warnings, and precise temperature control through an intelligent system. In warmer seasons, enhanced cooling measures are recommended, while in colder seasons, increased insulation is necessary. These adjustments significantly reduce temperature-induced stress risks. The research offers both theoretical foundations and practical guidance for temperature control during the construction of ultra-large volume concrete structures, thereby improving engineering quality and ensuring structural safety.

1. INTRODUCTION

In recent years, with the ongoing expansion of infrastructure construction, ultra-large volume concrete structures have been widely applied in major projects such as hydraulic engineering, transportation, energy, and high-rise buildings [1-3]. These structures, characterized by their large volumes and thick cross-sections, generate significant hydration heat during construction, causing rapid internal temperature increases. Due to concrete's relatively low thermal conductivity, heat within the structure is slow to dissipate, leading to large temperature gradients and thermal stresses, which can result in cracking and compromise the overall safety and integrity of the structure [4, 5]. Consequently, the dynamic analysis and effective control of hydration heat in ultra-large volume concrete have become critical technical challenges in the field of civil engineering.

The hardening process of concrete involves hydration reactions between cement and water, with the associated exothermic heat being the primary driver of temperature rise in large-volume concrete structures. The kinetics of hydration reactions-including reaction rates and cumulative heat release-are critically dependent on cement composition, mineral admixture ratios, and environmental temperature. Simultaneously, the evolution of internal temperature fields is governed by coupled heat transfer mechanisms encompassing thermal conduction, phase-change latent heat effects, and boundary heat dissipation conditions [6-8]. A systematic investigation of hydration thermodynamics in large-volume concrete is therefore essential for elucidating temperature evolution mechanisms and advancing intelligent thermal regulation technologies. While current engineering practices employ temperature control strategies such as embedded cooling pipes, layered casting techniques, and composite insulation systems [9, 10], significant challenges persist in adapting these methods to extreme thermal environments characterized by diverse geological conditions, climatic variations, and structural configurations.

Recent advancements in large-volume concrete hydration thermodynamics can be categorized into three key research domains: (1) Hydration heat generation mechanisms: Calorimetric studies have established modified Arrhenius equations and hyperbolic adiabatic temperature-rise models to quantify exothermic behavior in cement-admixture systems [11-14]. Experimental evidence demonstrates that 20% cement replacement with volcanic ash powder reduces peak exothermic output by 28% [15], while wood waste bottom ash incorporation induces distinct modifications to hydration heat release profiles [16]. Nevertheless, synergistic interactions in multi-component cementitious systems remain insufficiently characterized. (2) Temperature field prediction: Finite element-based thermo-mechanical coupling models reveal that incremental casting speed increases of 0.5 m/h elevate core temperature rise by 6-8℃ [17-20]. However, reconciling cost constraints with control efficiency remains a persistent technical challenge.

Therefore, using the Jinan Yellow River Fenghuang Bridge in China as a case study, analyzes the hydration heat dynamics of ultra-large volume concrete and the corresponding temperature control measures. It reveals the distribution patterns of temperature and stress in the joint sections and foundation slabs under different seasonal conditions and proposes cost-effective temperature control and crack prevention technologies. The findings provide both theoretical insights and practical guidance for optimizing temperature control during the construction of ultra-large volume concrete structures.

2. PROJECT OVERVIEW

The main bridge of the Jinan Yellow River Fenghuang Bridge in China is designed as a three-tower, self-anchored suspension bridge, featuring a main span of 2×428 m and a bridge deck width of 61.7 m. Both the span and bridge width are the largest in the world for this type of bridge. The bridge tower connection section adopts a wedge-shaped design, with maximum horizontal dimensions of 9 m × 12 m and a height of 11.22 m, constructed using C60 concrete, making it a large-volume concrete structure. The foundation slabs for the main piers 23# to 25# are rectangular, with dimensions of 33.2 m × 23.2 m and a height of 5 m, and are cast using C35 concrete. Both components are large-volume concrete structures, which share the common challenges of significant hydration heat, difficulty in crack control, and susceptibility to thermal cracking. Figure 1 illustrates the general construction details of the bridge tower connection section and foundation slab.

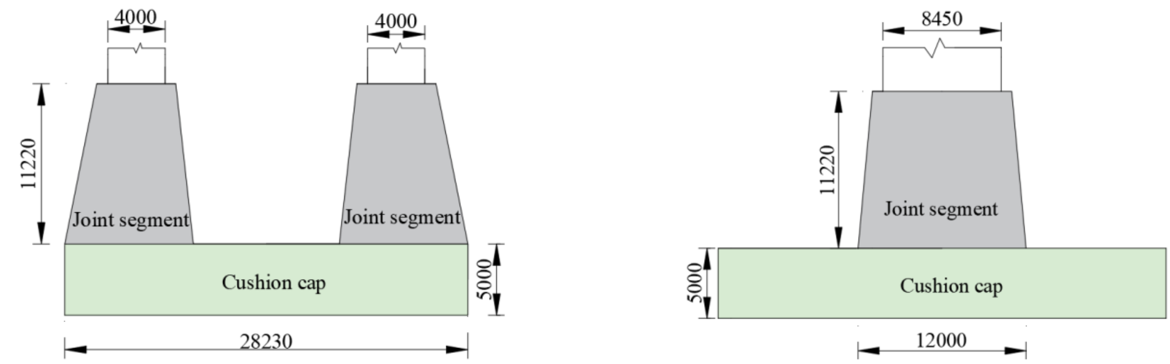

(a) Bridge tower connection section

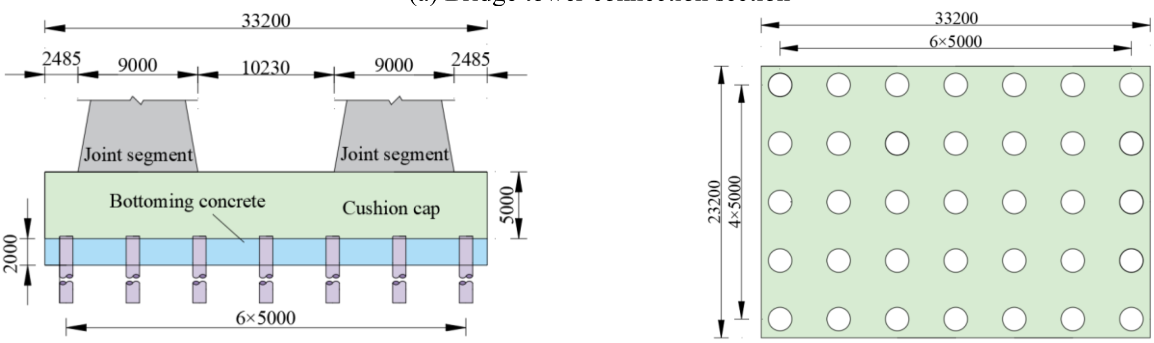

(b) Foundation slab

Figure 1. General construction details

The bridge site is located in Jinan, China, in the middle latitude zone. Influenced by solar radiation, atmospheric circulation, and the local geographical environment, the area has a warm temperate continental monsoon climate. During winter, Jinan is dominated by cold high-pressure systems from Mongolia, with northerly winds prevailing. Cold air masses typically invade every 6 to 8 days, causing a continuous drop in temperature. The average temperature in the coldest month is below 0℃, with extreme minimum temperatures averaging below -20℃. Days with temperatures below -10℃ account for 98% of the cold days, which are concentrated in the winter months. Winter precipitation ranges from 20 to 25 mm, constituting only 3.0% to 3.7% of the annual total. The winter season is marked by sparse rain and snow, frequent northerly winds, and dry, cold conditions.

3. POURING TEMPERATURE ANALYSIS

3.1 Theoretical analysis

The adiabatic temperature rise numerical model for the concrete of the bridge tower connection section and foundation slab is based on the following hyperbolic function:

$$Q(\tau) = Q_0(1-e^{-\alpha\tau^{\beta}}) \tag{1}$$

where, τ represents the age of the concrete when shrinkage begins, Q_0 is the final adiabatic temperature rise, and; α, β are the coefficients that describe the variation in the adiabatic temperature rise.

As time progresses, the elastic modulus is modeled using a four-parameter double-exponential function, i.e.,

$$E(\tau) = E_0 + \Delta E(1 - e^{-\alpha\tau^{\beta}}) \tag{2}$$

where, E_0 represents the initial elastic modulus; ΔE is the difference between the final elastic modulus E_2 and the initial elastic modulus, which is equal to E_2-E_0; and α, β denotes two parameters related to the rate of change in the elastic modulus.

Furthermore, the concrete creep factor is taken as

$$\begin{aligned} C(t,\tau) &= C_1(1+9.20\tau^{-0.45})(1-e^{-0.30(t-\tau)}) \\ &+ C_2(1+1.70\tau^{-0.45})(1-e^{-0.005(t-\tau)}) \end{aligned} \tag{3}$$

In the equation, C_1=0.23/E_2, C_2=0.52/E_2.

The equivalent heat release coefficient β_s for heat dissipation from the concrete surface to the surrounding medium through the insulation layer is calculated using the following formula:

$$\beta_s = \frac{1}{(1/\beta) + \sum\left(h_i/\lambda_i\right)} \tag{4}$$

where, β is the heat release coefficient, h_i is the thickness of the insulation layer in the i-th layer, and λ_i is the thermal conductivity of the insulation material in the i-th layer.

A 5mm steel plate insulation is applied to the side of the tower connection section. The equivalent heat release coefficient for the steel plate is denoted as 75.9KJ/m·h·℃, which is calculated using Eq. (4).

The thickness of the insulation layer is analyzed and calculated based on Eq. (5).

$$\delta = \frac{0.5h(T_S - T_q)\lambda_i}{\lambda_0(T_{\max} - T_b)} \cdot K_b \tag{5}$$

In the equation, δ represents the thickness of the concrete surface insulation layer, m; λ_0 is the thermal conductivity of concrete, W/(m·K), set at 2.33; λ_i is the thermal conductivity of the insulation material, W/(m·K), with geotextile selected for this project, taken as 0.06; T_s is the surface temperature of the concrete pouring body, ℃; T_q is the average atmospheric temperature when the concrete reaches its peak temperature 3 to 5 days after pouring, ℃; $T_s - T_q$ ranges from 15℃ to 20℃, with a value of 15℃; T_{max} is the maximum temperature inside the concrete pouring body, ℃; T_b is the surface temperature of the concrete, ℃; h is the actual thickness of the concrete structure, taken as 6.22 m; $T_{max} - T_b$ ranges from 20℃ to 25℃, with a value of 25℃; K_b is the heat transfer coefficient correction factor, set at 1.3.

Therefore, δ = 0.5×6.22×15×0.06×2/(2.33×25)=0.0625m. Thus, the thickness of the geotextile insulation should be greater than 62.5 mm.

3.2 Estimation of the pouring temperature

The concrete mix ratio for the bridge tower connection section (C60) is as follows: cement: fly ash: crushed stone: sand: water: admixture is equal to 425: 75: 1070: 713: 140: 6.5. For the foundation slab (C35), the mix ratio is: cement: fly ash: crushed stone: sand: water: admixture is equal to 300: 100: 1035: 811: 152: 4.4. Using local meteorological data and empirical temperature data for the raw materials, the concrete pouring temperatures for different months are estimated based on the reference mix ratios for the bridge tower connection section and foundation slab.

The construction period for the bridge tower connection section runs from August to October, while the foundation slab construction may extend across different months throughout the year. As a result, the year is divided into three periods to estimate the pouring temperatures. To control the temperature of raw materials, measures such as regulating cement temperature upon delivery and shading coarse aggregates will be implemented. Specifically, the cement temperature will be kept below 60℃, and the fly ash temperature will be maintained below 40℃. Table 1 presents the estimated pouring temperatures for both the bridge tower connection section and the foundation slab across different months.

Table 1. Concrete pouring temperatures for the bridge tower connection section and foundation slab across different months

Structural Component	Time	Average Ambient Temp. (℃)	Cement Temp. (℃)	Admixture Temp. (℃)	Aggregate Temp. (℃)	Water Temp. (℃)	Mold Insertion Temp. (℃)	Pouring Temp. (℃)
Connection section	Aug.	27.5	60	45	27	28	32.6	34.5
	Sep.	23.5	60	45	23	24	29.0	30.9
	Oct.	17.0	60	40	17	18	23.9	25.7
Foundation slab	Jan.	1.2	60	35	4	2	10.0	11.7
	Feb.	4.3	60	35	6	4	11.7	13.4
	Mar.	10.5	60	35	12	10	16.9	18.6
	Apr.	18.6	60	40	21	18	24.7	26.4
	May.	23.4	60	40	26	23	29.1	30.8
	Jun.	28.6	60	40	31	28	33.4	35.1
	Jul.	28.9	60	40	31	29	33.6	35.3
	Aug.	27.6	60	40	30	27	32.5	34.2
	Sep.	23.7	60	40	26	23	29.1	30.8
	Oct.	17.6	60	40	20	17	23.8	25.5
	Nov.	9.8	60	35	11	9	16.1	17.8
	Dec.	2.6	60	35	5	2	10.6	12.3

According to the construction schedule, the pouring period for the bridge tower connection section is from August to September. Based on the local temperature conditions, the average temperature during this period ranges from 23.5℃ to 27.5℃, resulting in an estimated pouring temperature for the C60 concrete of between 30.9℃ and 34.5℃. To ensure that the pouring temperature of the tower foundation and solid sections does not exceed 28℃, measures such as mixing crushed ice and using chilled water will be implemented. From December to February, which is the cold season in Jinan, the average temperature ranges from 1.2℃ to 4.3℃, with the foundation slab pouring temperature ranging from 11.7℃ to 13.4℃. During March, April, October, and November, Jinan experiences moderate temperatures, with average temperatures ranging from 9.8℃ to 18.6℃. The pouring temperature of the foundation slab is estimated to range from 17.8℃ to 26.7℃. In May and September, the high-temperature season in Jinan, the average temperature ranges from 23.4℃ to 28.9℃, and the foundation slab pouring temperature ranges from 30.8℃ to 35.3℃. To control the foundation slab pouring temperature and keep it below 28℃, measures such as mixing crushed ice and using chilled water will be implemented.

4. NUMERICAL SIMULATION AND RESULT ANALYSIS

4.1 Material parameters

Table 2 presents the physical and thermal parameters of the concrete used for the bridge tower connection section and foundation slab. The concrete mix design is initially determined through laboratory trials and trial mixes, ensuring that the concrete meets construction requirements such as workability, setting time, and other relevant factors. The concrete slump is controlled within the range of 180±20 mm.

Table 2. Physical and thermal properties of concrete in the bridge tower connection section and foundation slab

Strength Grade	Elastic Modulus (MPa)	28d Splitting Tensile Strength (MPa)	7d Hydration Heat of Cement (J/g)	Coefficient of Thermal Expansion (℃)	Thermal Conductivity (kJ/(m·d·℃)	Specific Heat (kJ/kg·℃)	Adiabatic Temp. Rise (℃)
C60	4.6×10^4	4.4	312	8×10^{-6}	228	0.89	56
C35	3.13×10^4	3.1	312	8×10^{-6}	228	0.92	44

4.2 Model establishment

ANSYS finite element analysis software is used for hydration heat analysis, carried out in two steps: Step 1 involves performing a temperature field analysis using temperature field elements to examine the hydration heat temperature distribution; Step 2 converts the temperature field results from Step 1 into a stress field, applies the corresponding boundary conditions, and then conducts the stress field analysis. The 3D solid element used for concrete is SOLID70, which has one temperature degree of freedom per node, heat conduction capability in all three directions, and allows for the transfer of uniform heat flow. This element is suitable for both 3D static and transient heat analysis, as well as structural analysis. The bridge tower connection section and foundation slab are modeled using 853 and 1239 elements, respectively. To take advantage of structural symmetry, the concrete models for the bridge tower connection section and foundation slab are reduced to 1/2 and 1/4 of the full geometry, respectively, for temperature and stress calculations.

4.3 Simulation calculation results

4.3.1 Bridge tower connection section

The bridge tower connection section is constructed using steel formwork, with a thickness of 4 to 5 mm. Based on the calculations, the surface heat dissipation coefficient is set at 75.9 kJ/(m²·h·℃). The concrete is poured in two stages, with cooling water pipes spaced 0.8 m apart horizontally, and the effect of these cooling pipes is included in the temperature calculations. Temperature and temperature stress calculations begin at the start of the concrete pouring, simulating the temperature and stress development over the subsequent 60 days. The pouring period for the bridge tower connection section is considered to be from August to September, with a pouring temperature of 28℃. The ambient temperature is based on the average maximum and minimum temperatures for Jinan in August, calculated as 28±4℃. Under these conditions, the highest internal temperature of the bridge tower connection section reaches 77.3℃, with the peak temperature occurring approximately 2 to 3 days after pouring. Figure 2 presents the simulation model for the connection section concrete and the temperature envelope showing the highest internal temperature, while the stress field is detailed in Figures 3(a) to 3(d).

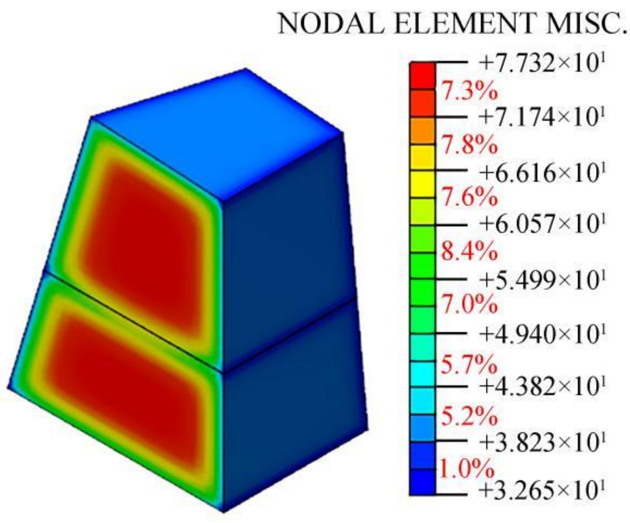

Figure 2. Simulation model of the connection section concrete and the envelope of the highest internal temperature

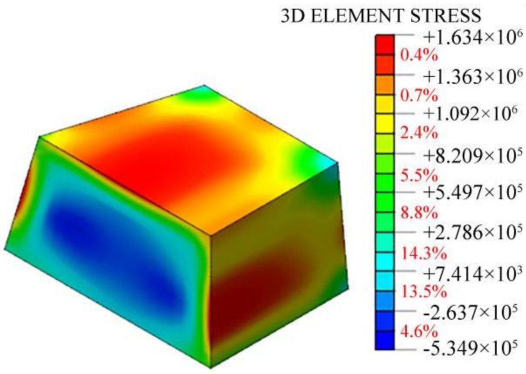

(a) The first layer, age 3d

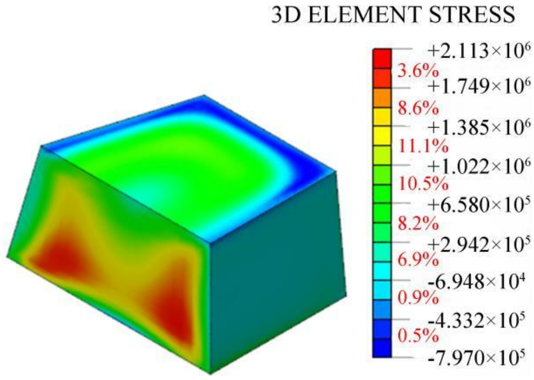

(b) The first layer, age 60d

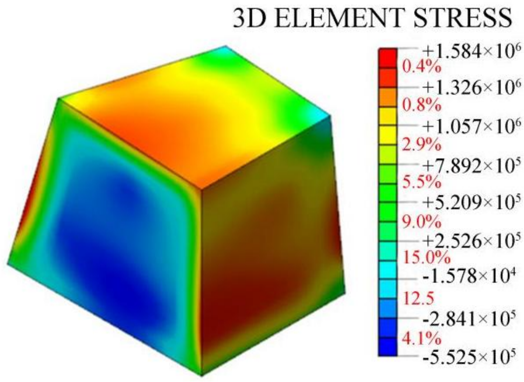

(c) The second layer, age 3d

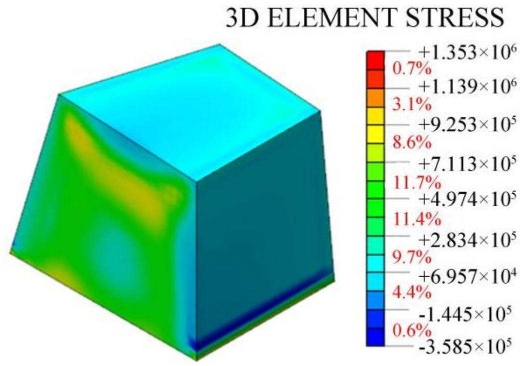

(d) The second layer, age 60d

Figure 3. Concrete temperature and stress fields at various ages for the bridge tower connection section

Table 3 presents the results of the temperature stress field calculations for the connection section during the cold season. A comparative analysis of the temperature stresses at different ages (3d, 7d, 28d, 60d) is conducted for both the first and second layers. The results indicate that the temperature stress in the first layer is 1.63 MPa at 3 days, gradually increasing to 2.63 MPa at 7 days, reaching a peak of 3.01 MPa at 28 days, and then decreasing to 2.11 MPa at 60 days. In contrast, the stress variation in the second layer is more gradual, with values of 1.59 MPa at 3 days and 2.52 MPa at 7 days. After 28 days, the stress decreases significantly, with values of 1.43 MPa at 28 days and 1.35 MPa at 60 days. The safety factor calculated for all cases is no less than 1.35. Overall, the temperature stress in the first layer exhibits a larger fluctuation over time and remains higher than in the second layer, suggesting that the first layer is more significantly affected by temperature changes during the cold season. The splitting tensile strength values for the cold season are 2.2 MPa, 3.6 MPa, 4.4 MPa, and 4.6 MPa at 3d, 7d, 28d, and 60d, respectively.

Table 3. Calculation results of the temperature stress field for the bridge tower connection section in the cold season

Operating Condition	Structural Component	3d	7d	28d	60d
Low-temperature season	The first layer	1.63	2.63	3.01	2.11
	The second layer	1.59	2.52	1.43	1.35

4.3.2 Foundation slab

The foundation slab is constructed using a steel sheet piling enclosure and steel formwork, with the formwork thickness ranging from 4 to 5 mm. Based on calculations, the surface heat dissipation coefficient is taken as 75.9 kJ/(m²·h·°C). The concrete for the foundation slab is poured in two stages along the thickness direction: the first stage is 2 meters, and the second stage is 3 meters. A total of five layers of cooling water pipes are arranged, with the horizontal spacing between the pipes set at 1.0 meter, and the effect of the cooling pipes is incorporated into the calculations. The temperature and temperature stress calculations begin at the start of concrete pouring, simulating the development of temperature and stress over the next 60 days.

The analysis is divided into three scenarios. For the low-temperature season, the concrete pouring for the foundation slab is considered to take place from December to February, with a pouring temperature of 14°C and an ambient temperature of 5±4°C. For the normal-temperature season, the pouring is considered to occur in March, April, October, and November, with a pouring temperature of 27°C and an ambient temperature of 16±4°C. For the high-temperature season, the pouring is considered to occur from May to September, with a pouring temperature of 28°C and an ambient temperature of 28±4°C.

Under the conditions of the low, normal, and high-temperature seasons, the highest internal temperatures of the foundation slab are 49.7°C, 62.6°C, and 64.3°C, respectively, with the peak temperature occurring around 3 to 4 days after pouring. The temperature envelope showing the highest internal temperatures of the foundation slab is presented in Figure 4(a) to (c), and the stress calculation results are shown in Table 4. The stress field for the low-temperature season is illustrated in Figure 5.

Table 4 presents the calculated results of the temperature stress field for the foundation slab under different seasonal conditions. It analyzes the temperature stress variation trends for the first and second layers at ages of 3, 7, 28, and 60 days.

In the cold season, the temperature stress for both the first and second layers generally increases with age. At 60 days, the stress in the first layer reaches 2.22 MPa, while the second layer reaches 2.39 MPa, slightly higher than the first layer.

In the normal temperature season, the stress variation trend for both layers is similar to that in the cold season, but the overall stress values are slightly higher. Notably, the stress in the second layer reaches 2.40 MPa at 60 days, the highest observed value.

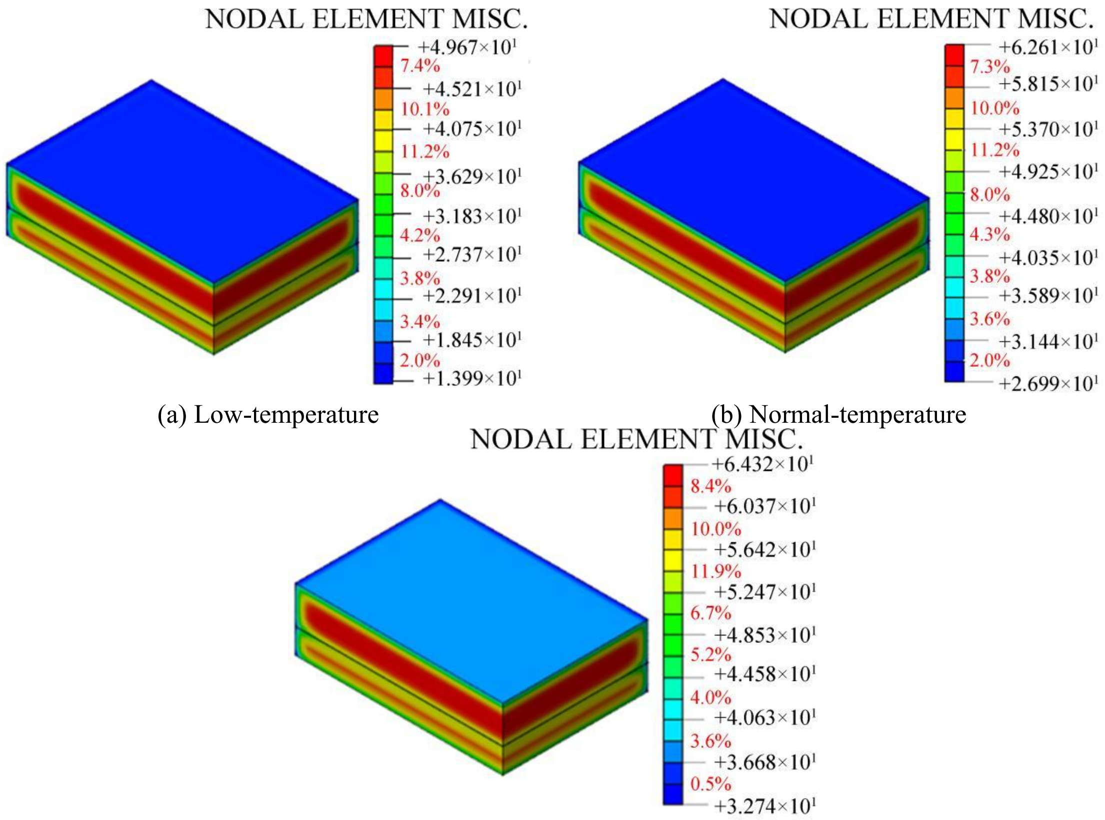

(a) Low-temperature (b) Normal-temperature

(c) High-temperature

Figure 4. Temperature envelope of the highest internal temperature of the foundation slab concrete in different seasons

Table 4. Calculation results of the temperature stress field for the foundation slab under various seasonal conditions

Operating Condition	Structural Component	3d	7d	28d	60d
Low-temperature season	The first layer	1.22	1.62	2.01	2.22
	The second layer	1.24	1.7	2.11	2.39
Normal-temperature season	The first layer	1.18	1.62	2.12	2.34
	The second layer	1.21	1.61	2.12	2.40
High-temperature season	The first layer	1.18	1.00	1.50	2.20
	The second layer	1.14	1.54	1.70	2.25

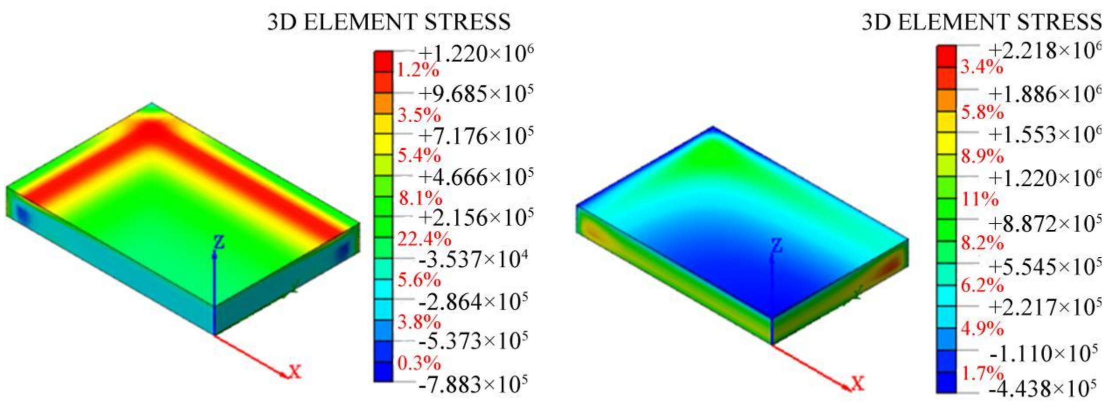

(a) The first layer, age 3d (b) The first layer, age 60d

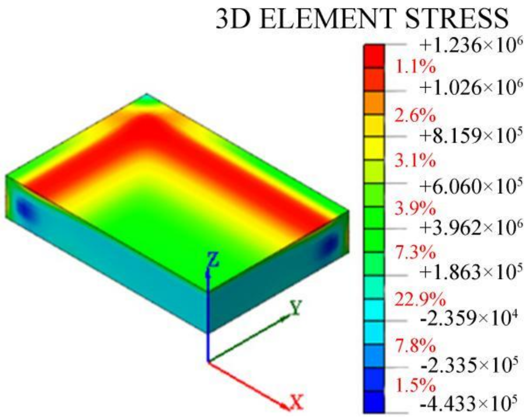

(c) The second layer, age 3d

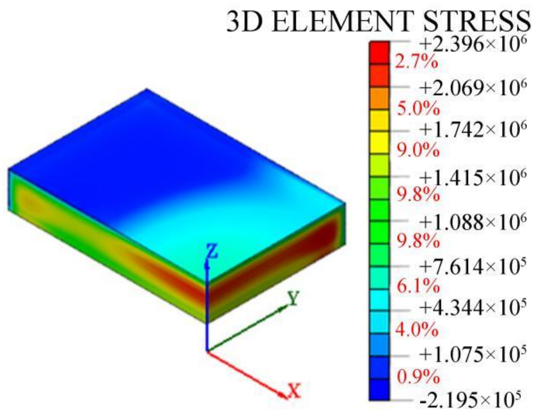

(d) The second layer, age 60d

Figure 5. Concrete temperature and stress field at various ages for the foundation slab in the cold season

In the high-temperature season, the temperature stress shows significant fluctuations. The first layer experiences lower stress at early (3 days) and mid (7 days) stages, with values of 1.18 MPa and 1.00 MPa, respectively. However, the stress increases rapidly in the later stages (28 days and 60 days), reaching 1.50 MPa and 2.20 MPa, respectively. The stress variation in the second layer is relatively stable, gradually increasing from 3 days to 60 days, reaching 2.25 MPa. The calculated safety factor is approximately 1.37 for all cases.

Overall, the stress growth patterns for the foundation slab in the cold and normal temperature seasons are quite similar, whereas the high-temperature season shows lower early-stage stress with rapid growth in later stages. This indicates that temperature control measures need to be optimized according to seasonal variations. Throughout the year, the splitting tensile strength values are 1.7 MPa, 2.4 MPa, 3.1 MPa, and 3.5 MPa at 3, 7, 28, and 60 days, respectively.

5. INTELLIGENT TEMPERATURE CONTROL SYSTEM AND PERFORMANCE COMPARISON

5.1 Intelligent temperature control system

The concrete intelligent monitoring system proposed in this paper is an integrated intelligent temperature control solution, developed by combining a wireless monitoring module, an intelligent pipe cooling module, and an intelligent curing module. The system incorporates capabilities for data analysis, information push and early warnings, automatic control, and remote monitoring, all designed to optimize concrete temperature control and significantly reduce the risk of cracking. Key features of the system include wireless data collection, a data processing platform, online platform notifications and alerts, and intelligent control mechanism.

The system provides scientific references for parameter adjustment and measure formulation by comparing and analyzing construction methods and temperature control data for similar structures in the same region, in conjunction with optimization solutions derived from finite element simulations. Additionally, by utilizing wireless automatic monitoring equipment, the system enables real-time data monitoring and automatic early warnings. Users can access data in real-time through WeChat and PC clients, and receive alerts for key parameters, ensuring full control over on-site temperature conditions. Furthermore, the system platform supports identity authentication and hierarchical management, delivering personalized data based on user needs and enabling a closed feedback loop through online responses, which enhances issue resolution speed. Lastly, the intelligent temperature control system integrates proprietary pipe cooling circulation and curing modules, offering high-precision flow control. It allows for real-time adjustments based on platform data, overcoming the delays and inaccuracies typically associated with manual interventions.

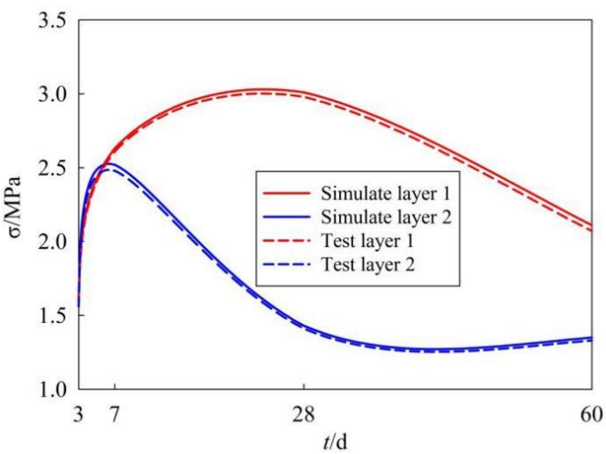

(a) Bridge tower connection section low-temp season

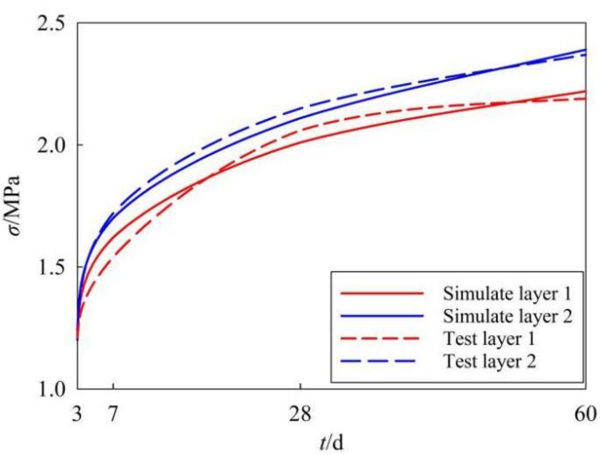

(b) Foundation slab low-temperature season

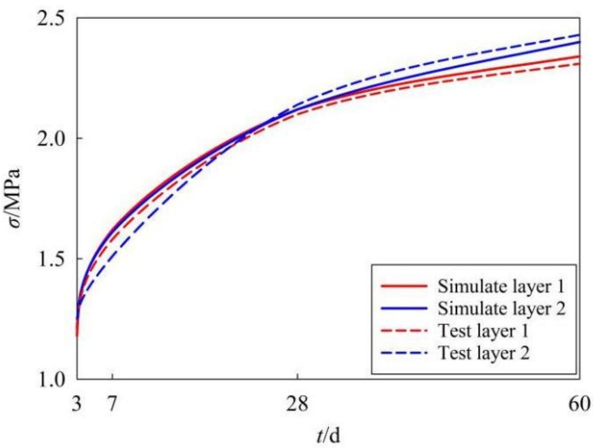

(c) Foundation slab normal-temperature season

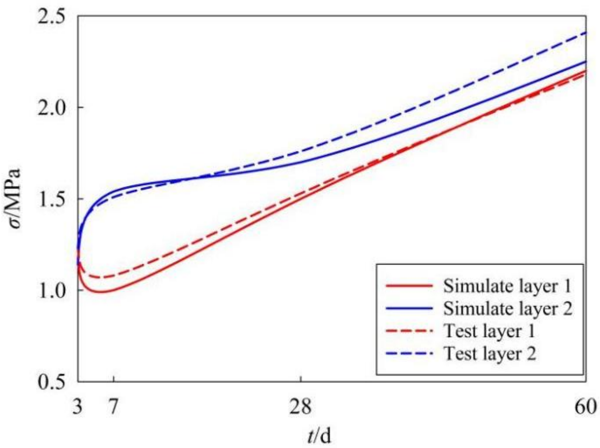

(d) Foundation slab high-temperature season

Figure 6. Comparison of experimental and numerical simulation results

5.2 Comparison of temperature control effects

Temperature and stress sensors are installed in the bridge tower concrete connection section and foundation slab, with the cooling pipe temperature regulated through the concrete intelligent monitoring system. Figure 6 presents a comparison of the experimental and numerical simulation results. By analyzing the experimental and simulation data, the accuracy and applicability of the numerical model can be clearly evaluated. In this study, the experimental results and simulation data exhibit consistent trends in key indicators, indicating that the numerical model accurately reflects the dynamic behavior of concrete hydration heat. Under varying temperature conditions, the maximum discrepancy between the experimental and simulation results is 2%, which may be attributed to boundary condition settings and mesh refinement. Overall, the experimental data confirm the reliability of the numerical simulation, providing strong support for the widespread application of the concrete intelligent monitoring system.

6. CONCLUSION

This paper uses the Jinan Yellow River Fenghuang Bridge in China as a case study to develop a hydration heat dynamic model suitable for various engineering conditions. The study identifies key factors influencing the temperature and stress fields in large-volume concrete and proposes cost-effective temperature control and crack prevention techniques. The main findings are as follows:

(1) Based on the seasonal temperature characteristics in Jinan, targeted temperature control measures are proposed. During the high-temperature season and under high pouring temperature conditions, cooling measures such as the use of crushed ice and chilled water are necessary, and the pouring temperature must be strictly controlled to not exceed 28℃. In contrast, during the cold season, insulation measures should be implemented to maintain construction quality. These measures effectively reduce temperature-induced stress risks and prevent harmful cracking.

(2) The temperature stress in the bridge tower connection section during the cold season shows clear trends with age. The temperature stress in the first layer fluctuates more significantly and is consistently higher than in the second layer, indicating that the low-temperature environment has a more pronounced impact on the first layer. Additionally, the splitting tensile strength at all ages meets safety requirements, with safety factors no less than 1.35, confirming the rationality of the structural design.

(3) The temperature stress variation in the foundation slab is heavily influenced by seasonal factors. During the cold and normal-temperature seasons, the temperature stress increases gradually with age, and the stress distribution remains relatively uniform. In contrast, the high-temperature season exhibits lower stress in the early stages, followed by rapid growth in the later stages, highlighting the need for enhanced temperature control measures to maintain construction quality during hot weather.

(4) The comparison of experimental data with numerical simulation results shows consistent trends in key indicators, with a maximum error of only 5%. This demonstrates that the numerical model accurately reflects the dynamic behavior of concrete hydration heat. These results provide essential reference for the design and optimization of temperature control systems and lay a solid theoretical foundation for their application in large-volume concrete construction.

(5) The concrete intelligent temperature control system, which combines wireless monitoring, data comparative analysis, and automated regulation, enables real-time monitoring of on-site temperature changes and provides early warnings. This improves construction efficiency and safety. The system's high-precision flow control module significantly reduces the lag associated with manual adjustments, further optimizing the temperature control effect.

REFERENCES

[1] Potuckova, S., Holy, M., Kolisko, J. (2024). The impact of hydration heat on the formation of cracks in massive concrete structures. Key Engineering Materials, 976: 121-128. https://doi.org/10.4028/p-IJ4KhU

[2] Orozco, C., Tangtermsirikul, S., Sugiyama, T., Babel, S. (2024). Unraveling the environmental and economic impacts of fly ash utilization on mass concrete considering industry practices. Journal of Material Cycles and Waste Management, 26(3): 1403-1417. https://doi.org/10.1007/s10163-024-01893-y

[3] Korda, E., De Schutter, G., Aggelis, D.G. (2024).

Acoustic signatures of hydration and microcracking in early-age concrete. Developments in the Built Environment, 17: 100353. https://doi.org/10.1016/j.dibe.2024.100353

[4] Klemczak, B., Smolana, A. (2024). Multi-step procedure for predicting early-age thermal cracking risk in mass concrete structures. Materials, 17(15): 3700. https://doi.org/10.3390/ma17153700

[5] Singh, M.P., Sen, S., Pathak, H., Dogra, A.B. (2024). Early age cracking relevant to mass concrete dam structures during the construction schedule. Construction and Building Materials, 411: 134739. https://doi.org/10.1016/j.conbuildmat.2023.134739

[6] de Souza, M.H.B., Silva, L.R.R., Ribeiro, V.A.D.S., Gonçalves, P.C., Melo, M.D.L.N.M., Gomes, C.E.M., dos Santos, V.C. (2023). Influence of superabsorbent polymer in self-compacting mortar. Buildings, 13(7): 1640. https://doi.org/10.3390/buildings13071640

[7] Abolhasani, A., Samali, B., Aslani, F. (2022). Rice husk ash incorporation in calcium aluminate cement concrete: Life cycle assessment, hydration and strength development. Sustainability, 14(2): 1012. https://doi.org/10.3390/su14021012

[8] Pizoń, J., Łaźniewska-Piekarczyk, B., Miera, P. (2022). The influence of the acceleration admixture type and composition of cement on hydration heat and setting time of slag blended cement. Materials, 15(8): 2797. https://doi.org/10.3390/ma15082797

[9] Meh, K.M.F.K., Jamellodin, Z., Salleh, N., Hamid, N.A.A., Adnan, S.H. (2022). Effect of palm oil fuel ash and eggshell waste powder on compressive strength and heat of hydration for concrete. In IOP Conference Series: Earth and Environmental Science, 1022(1): 012050. https://doi.org/10.1088/1755-1315/1022/1/012050

[10] Ghosh, R., Lahoti, M., Shah, B. (2022). A succinct review on the use of NMR spectroscopy in monitoring hydration, strength development, and inspection of concrete. Materials Today: Proceedings, 61: 167-173. https://doi.org/10.1016/j.matpr.2021.07.433

[11] Al-Hasani, L.E., Perez, G., Herndon, H.N., Park, J., Poole, J.L., Tien, I., Kurtis, K.E. (2023). Prediction of heat of hydration of cementitious systems using Gaussian process regression enables mass concrete thermal modeling. Materials and Structures, 56(2): 45. https://doi.org/10.1617/s11527-023-02134-8

[12] Kang, H., Moon, J. (2021). Secondary curing effect on the hydration of ultra-high performance concrete. Construction and Building Materials, 298: 123874. https://doi.org/10.1016/j.conbuildmat.2021.123874

[13] Ghoddousi, P., Salehi, A.M., Shirzadi Javid, A.A., Etebari Ghasbeh, M.A., Sajjadi, S. (2023). Evaluation of concrete bulk resistivity as the key performance index for chloride transport in concrete and rate of hydration. International Journal of Civil Engineering, 21(3): 507-522. https://doi.org/10.1007/s40999-022-00786-1

[14] Kiernożycki, W., Błyszko, J. (2021). The influence of temperature on the hydration rate of cements based on calorimetric measurements. Materials, 14(11): 3025. https://doi.org/10.3390/ma14113025

[15] Alhozaimy, A., Fares, G., Alawad, O.A., Al-Negheimish, A. (2015). Heat of hydration of concrete containing powdered scoria rock as a natural pozzolanic material. Construction and Building Materials, 81: 113-119. https://doi.org/10.1016/j.conbuildmat.2015.02.011

[16] Vaičienė, M., Malaiškienė, J., Maqbool, Q. (2023). The impact of milled wood waste bottom ash (WWBA) on the properties of conventional concrete and cement hydration. Materials, 16(19): 6498. https://doi.org/10.3390/ma16196498

[17] Lopes, A.V., Lopes, S.M. (2024). New methodology for evaluating strength degradation from temperature increase in concrete hydration under adiabatic conditions. Materials, 17(19): 4830. https://doi.org/10.3390/ma17194830

[18] Castilho, E., Schclar, N., Tiago, C., Farinha, M.L.B. (2018). FEA model for the simulation of the hydration process and temperature evolution during the concreting of an arch dam. Engineering Structures, 174: 165-177. https://doi.org/10.1016/j.engstruct.2018.07.065

[19] Tahersima, M., Tikalsky, P. (2017). Finite element modeling of hydration heat in a concrete slab-on-grade floor with limestone blended cement. Construction and Building Materials, 154: 44-50. https://doi.org/10.1016/j.conbuildmat.2017.07.176

[20] Bourchy, A., Barnes, L., Bessette, L., Chalencon, F., Joron, A., Torrenti, J.M. (2019). Optimization of concrete mix design to account for strength and hydration heat in massive concrete structures. Cement and Concrete Composites, 103: 233-241. https://doi.org/10.1016/j.cemconcomp.2019.05.005